Spiral diffusion imaging at 800 μm resolution using a scanner with 300 mT/m gradients and gradient field monitoring

Luke Joel Edwards[1], Kerrin J. Pine[1], Shubhajit Paul[1], Fakhereh Movahedian Attar[1], Michael Herbst[2], Mirsad Mahmutović[3], Boris Keil[3], Harald Möller[4], Evgeniya Kirilina[1,5], and Nikolaus Weiskopf[1,6]

[1]Department of Neurophysics, Max Planck Institute for Human Cognitive and Brain Sciences, Leipzig, Germany, [2]Gengenbach, Germany, [3]Institute of Medical Physics and Radiation Protection, TH Mittelhessen University of Applied Sciences, Giessen, Germany, [4]NMR Group, Max Planck Institute for Human Cognitive and Brain Sciences, Leipzig, Germany, [5]Center for Cognitive Neuroscience Berlin, Freie Universität Berlin, Berlin, Germany, [6]Felix Bloch Institute for Solid State Physics, Leipzig University, Leipzig, Germany

Synopsis

Spiral diffusion weighted imaging (DWI) with field monitoring and iterative reconstruction offers potentially reduced echo time (TE) and higher effective resolution (less blurring) compared to EPI. Coupled with a scanner with ultra-strong gradients, it enabled an 800 μm DWI protocol for imaging fine structures of the brain in vivo. Compared to EPI, the shorter TEs provided distinctly different contrast in iron-rich areas (U-fibres and sub-cortical nuclei), which could enhance investigations of these regions. The protocol did, however, come with a reduction in SNR/(unit time) compared to EPI due to differences in readout time.

Introduction

Diffusion weighted imaging (DWI) of brain tissue allows access to microstructural properties of brain in vivo[1]. However, high resolution is required to separate and segment fine structures like cortex[2], sub-cortical nuclei[3], or U-fibres[4].

Spiral trajectories are more efficient than rectilinear k-space trajectories[5] and enable shorter effective echo time[6,7,8] (TE). Shorter TEs retain higher signal levels and increase the range of TEs that can be sampled. Importantly, varying TE can provide additional microstructural information[9,10]. This is especially pertinent for U-fibres and deep gray matter, because their high relative iron content[11,12] means that behaviour in the low TE-regime is likely to be interesting.

MRI scanners with ultra-strong gradients have recently enabled enhanced in vivo DWI U-fibre imaging in lower visual areas using a protocol optimised for the occipital lobe[4]. Here, we demonstrate the potential of spiral acquisitions to allow for shorter TE in this protocol, while ensuring high image quality using field monitoring and iterative reconstruction.

Methods

Data were recorded from a young healthy participant on a Siemens Connectom 3T scanner with a 32-channel receive-only head coil.

Spiral data: spin echo DWI sequence with spiral readout[13]; TE 33 ms; TR 6500 ms; 800 μm isotropic resolution; 220×220 mm^2 field of view (FoV); 62 slices; oblique axial, tilted along the calcarine sulcus; 41 ms readout time; bandwidth (BW) 952 Hz/px; 4× radially undersampled; acquisition repeated 4× with initial azimuthal phase $(n-1)\pi/2$ (4 arms); $b = 8, 18$ ms/μm^2; 60 non-colinear directions per shell distributed over the sphere; 15 interleaved $b = 0$ ms/μm^2 (b_0) volumes; total acquisition time (TA) ~1hr. Multi-echo GRE images were recorded at 1.5 mm isotropic resolution to calculate B0 and coil sensitivity maps, TA ~3mins. Additionally, $20 \times b_0$ images were recorded for temporal signal-to-noise ratio (tSNR) comparison with EPI, TA ~9mins.

The spiral trajectory was measured up to spatial second-order[14] in a separate calibration on a phantom using a 64-channel receive-only head coil[15,16] with built in field monitoring probes connected to a field monitoring system (Skope Magnetic Resonance Technologies).

Spiral data were reconstructed using iterative SENSE reconstruction in the Skope-i software (Skope Magnetic Resonance Technologies), incorporating the recorded trajectories and the B0 and coil-sensitivity maps[14]. Spiral arms were combined using an implementation of MUSE[17] in Skope-i. Scanner-side eddy current correction[18] was removed before reconstruction using simulations of the trajectory (https://github.com /SkopeMagneticResonanceTechnologies/siemens_to_ismrmrd) so that the measured values could be used.

EPI data: measured in a separate session and previously published[4]. Parameters different from spiral acquisition: spin echo EPI sequence[16,19]; TE 66 ms; TR 8900 ms; 206×206 mm^2 FoV; 81 ms readout time; BW 1148 Hz/px; GRAPPA[20] 2; partial Fourier 5/8; two repetitions; one additional b_0 image with opposed phase encoding recorded for susceptibility correction[21,22]; total TA ~45mins. In addition, one repetition of $20 \times b_0$ images were recorded in the same session as the spiral for tSNR comparison, TA ~5mins.

DWI data were preprocessed as per Attar, et al.[4], except that because eddy current and susceptibility corrections are incorporated into the spiral reconstruction, in that case these steps were replaced with correction for inter-volume motion using the ACID toolbox[23]. Diffusion tensors[24], and multi-tissue CSD segmentations and fibre orientation distribution functions[25] (fODFs) were computed from the DWI data using MRtrix3[26].

The b_0 data for tSNR comparison was not preprocessed. tSNR was computed voxelwise over the b_0 repetitions as (signal mean)/(signal standard deviation). Separately for spiral and EPI images, the mean b_0 image was segmented using SPM12, and white matter (WM) probability maps were thresholded at 99% to generate WM masks. The distribution of tSNR was compared in these WM masks.

Results

Fig. 1 demonstrates that the spiral acquisition gives higher effective spatial resolution in terms of crisper delineation of tissue classes and less blurring. It also suggests that the shorter TE for the spiral gives differential sensitivity to U-fibres, in line with their increased iron content[12].

The tSNR comparison (Fig. 2) demonstrated comparable tSNR for 4-arm spiral and single-repetition EPI. Over the WM, spiral tSNR (mean $\pm$ standard deviation) was 4.5 ± 1.6 in ~9mins, EPI tSNR 4.7 ± 1.3 in ~5mins. The distribution of tSNR was seen to be flatter for the spiral, in line with previous results[7], though this may be in part due to the lack of susceptibility correction in the EPI case. The effect of the shorter TE on deep gray matter contrast was also apparent.

Discussion and Conclusion

Unlike in previous work[7], our spiral acquisition was less SNR/(unit time) efficient than the EPI. The main reason for this is that the EPI has a readout time twice as long as the spiral. A further contributing factor is that the partial Fourier encoding leads to blurring and thus a lower effective resolution in the phase-encoding direction of the EPI. However, two repetitions of the EPI protocol can be run in the same time as the spiral protocol.

On the other hand, the spiral DWI offered a higher (and isotropic) effective resolution and shorter minimal TE, though the contributions of TE, field monitoring, and iterative reconstruction to the higher resolution remain to be disentangled. Spiral DWI holds the potential to enhance investigations of diffusion properties of thin and small structures like cortex, U-fibres, and deep grey matter nuclei in vivo in the low TE-regime at sub-millimetre resolution.

Acknowledgements

References

[1] Alexander, D.C., Dyrby, T.B., Nilsson, M., Zhang, H. (2019), "Imaging brain microstructure with diffusion MRI: practicality and applications", NMR Biomed. https://doi.org/10.1002/nbm.3841

[2] Edwards, L.J., Kirilina, E., Mohammadi, S., Weiskopf, N. (2018), "Microstructural imaging of human neocortex in vivo", Neuroimage. https://doi.org/10.1016/j.neuroimage.2018.02.055

[3] Keuken, M.C., Bazin, P.-L., Crown, L., Hootsmans, J., Laufer, A., Müller-Axt, C., Sier, R., van der Putten, E.J., Schäfer, A., Turner, R., Forstmann, B.U. (2014), "Quantifying inter-individual anatomical variability in the subcortex using 7T structural MRI", Neuroimage. https://doi.org/10.1016/j.neuroimage.2014.03.032

[4] Movahedian Attar, F., Kirilina, E., Haenelt, D., Pine, K.J., Trampel, R., Edwards, L.J., Weiskopf, N. (2020), "Mapping Short Association Fibers in the Early Cortical Visual Processing Stream Using In Vivo Diffusion Tractography", Cereb. Cortex. https://doi.org/10.1093/cercor/bhaa049

[5] Delattre, B.M.A., Heidemann, R.M., Crowe, L.A., Vallée, J.-P., Hyacinthe, J.-N. (2010), "Spiral demystified", Magn. Reson. Imaging. https://doi.org/10.1016/j.mri.2010.03.036

[6] Mueller, L., Rudrapatna, S.U., Tax, C.M.W., Wise, R., Jones D.K. (2019), "Diffusion MRI with b=1000 s/mm2 at TE < 22 ms using single-shot spiral readout and ultra-strong gradients: Implications for microstructure imaging", Proc. Int. Soc. Magn. Reson. Med.

[7] Lee, Y., Wilm, B.J., Brunner, D.O., Gross, S., Schmid, T., Nagy, Z., Pruessmann, K.P. (2020), "On the signal-to-noise ratio benefit of spiral acquisition in diffusion MRI". Magn. Reson. Med. https://doi.org/10.1002/mrm.28554

[8] Wilm, B.J., Hennel, F., Roesler, M.B., Weiger, M., Pruessmann, K.P. (2020), "Minimizing the echo time in diffusion imaging using spiral readouts and a head gradient system", Magn Reson Med. https://doi.org/10.1002/mrm.28346

[9] Jones, D.K., Alexander, D.C., Bowtell, R., Cercignani, M., Dell'Acqua, F., McHugh, D.J., Miller, K.L., Palombo, M., Parker, G.J.M., Rudrapatna, U.S., Tax, C.M.W. (2018), "Microstructural imaging of the human brain with a 'super-scanner': 10 key advantages of ultra-strong gradients for diffusion MRI", Neuroimage. https://doi.org/10.1016/j.neuroimage.2018.05.047

[10] Barakovic, M., Tax, C.M.W., Rudrapatna, U.S., Chamberland, M., Rafael-Patino, J., Granziera, C., Thiran, J.P., Daducci, A., Canales-Rodríguez, E.J., Jones, D.K. (2020), "Resolving bundle-specific intra-axonal T2 values within a voxel using diffusion-relaxation tract-based estimation", Neuroimage. https://doi.org/10.1016/j.neuroimage.2020.117617

[11] Deistung, A., Schäfer, A., Schweser, F., Biedermann, U., Turner, R., Reichenbach, J.R. (2013), "Toward in vivo histology: A comparison of quantitative susceptibility mapping (QSM) with magnitude-, phase-, and R2*-imaging at ultra-high magnetic field strength", Neuroimage. https://doi.org/10.1016/j.neuroimage.2012.09.055

[12] Kirilina, E., Helbling, S., Morawski, M., Pine, K., Reimann, K., Jankuhn, S., Dinse, J., Deistung, A., Reichenbach, J.R., Trampel, R., Geyer, S., Müller, L., Jakubowski, N., Arendt, T., Bazin, P.-L., Weiskopf, N. (2020), "Superficial white matter imaging: Contrast mechanisms and whole-brain in vivo mapping", Sci. Adv. https://doi.org/10.1126/sciadv.aaz9281

[13] Herbst, M., Deng, W., Ernst, T. and Stenger, V.A. (2017), "Segmented simultaneous multi-slice diffusion weighted imaging with generalized trajectories", Magn. Reson. Med. https://doi.org/10.1002/mrm.26545

[14] Wilm, B.J., Barmet, C., Pavan, M. and Pruessmann, K.P. (2011), "Higher order reconstruction for MRI in the presence of spatiotemporal field perturbations", Magn. Reson. Med. https://doi.org/10.1002/mrm.22767

[15] Keil, B., Blau, J.N., Biber, S., Hoecht, P., Tountcheva, V., Setsompop, K., Triantafyllou, C. and Wald, L.L. (2013), "A 64-channel 3T array coil for accelerated brain MRI". Magn. Reson. Med. https://doi.org/10.1002/mrm.24427

[16] Setsompop, K., Kimmlingen, R., Eberlein, E., Witzel, T., Cohen-Adad, J., McNab, J.A., Keil, B., Tisdall, M.D., Hoecht, P., Dietz, P., Cauley, S.F., Tountcheva, V., Matschl, V., Lenz, V.H., Heberlein, K., Potthast, A., Thein, H., Van Horn, J., Toga, A., Schmitt, F., Lehne, D., Rosen, B.R., Wedeen, V., Wald, L.L. (2013), "Pushing the limits of in vivo diffusion MRI for the Human Connectome Project", Neuroimage. https://doi.org/10.1016/j.neuroimage.2013.05.078

[17] Chen, N.-k., Guidon, A., Chang, H.-C., Song, A.W., (2013), "A robust multi-shot scan strategy for high-resolution diffusion weighted MRI enabled by multiplexed sensitivity-encoding (MUSE)", Neuroimage. https://doi.org/10.1016/j.neuroimage.2013.01.038

[18] Ma, R., Akçakaya, M., Moeller, S., Auerbach, E., Uğurbil, K., Van de Moortele, P.-F. (2020), "A field-monitoring-based approach for correcting eddy-current-induced artifacts of up to the 2nd spatial order in human-connectome-project-style multiband diffusion MRI experiment at 7T: A pilot study", Neuroimage. https://doi.org/10.1016/j.neuroimage.2020.116861

[19] Setsompop, K., Cohen-Adad, J., Gagoski, B.A., Raij, T., Yendiki, A., Keil, B., Wedeen, V.J., Wald, L.L. (2012), "Improving diffusion MRI using simultaneous multi-slice echo planar imaging", Neuroimage. https://doi.org/10.1016/j.neuroimage.2012.06.033

[20] Griswold, M.A., Jakob, P.M., Heidemann, R.M., Nittka, M., Jellus, V., Wang, J., Kiefer, B. and Haase, A. (2002), "Generalized autocalibrating partially parallel acquisitions (GRAPPA)", Magn. Reson. Med. https://doi.org/10.1002/mrm.10171

[21] Andersson, J. L. Skare, S., Ashburner, J. (2003), "How to correct susceptibility distortions in spin-echo echo-planar images: application to diffusion tensor imaging", Neuroimage. https://doi.org/10.1016/S1053-8119(03)00336-7

[22] Smith, S.M., Jenkinson, M., Woolrich, M.W., Beckmann, C.F., Behrens, T.E., Johansen-Berg, H., Bannister, P.R., De Luca, M., Drobnjak, I., Flitney, D.E., Niazy, R.K., Saunders, J., Vickers, J., Zhang, Y., De Stefano, N., Brady, J.M., Matthews, P.M. "Advances in functional and structural MR image analysis and implementation as FSL", Neuroimage. https://doi.org/10.1016/j.neuroimage.2004.07.051

[23] Mohammadi, S., Möller, H.E., Kugel, H., Müller, D.K. and Deppe, M. (2010), "Correcting eddy current and motion effects by affine whole-brain registrations: Evaluation of three-dimensional distortions and comparison with slicewise correction", Magn. Reson. Med. https://doi.org/10.1002/mrm.22501

[24] Veraart, J., Sijbers, J., Sunaert, S., Leemans, A., Jeurissen, B. (2013), "Weighted linear least squares estimation of diffusion MRI parameters: Strengths, limitations, and pitfalls", Neuroimage. https://doi.org/10.1016/j.neuroimage.2013.05.028

[25] Jeurissen, B., Tournier, J.-D., Dhollander, T., Connelly, A., Sijbers, J. (2014), "Multi-tissue constrained spherical deconvolution for improved analysis of multi-shell diffusion MRI data", Neuroimage. https://doi.org/10.1016/j.neuroimage.2014.07.061

[26] Tournier, J.D., Smith, R., Raffelt, D., Tabbara, R., Dhollander, T., Pietsch, M., Christiaens, D., Jeurissen, B., Yeh, C.-H., Connelly, A. (2019) "MRtrix3: A fast, flexible and open software framework for medical image processing and visualisation", Neuroimage. https://doi.org/10.1016/j.neuroimage.2019.116137
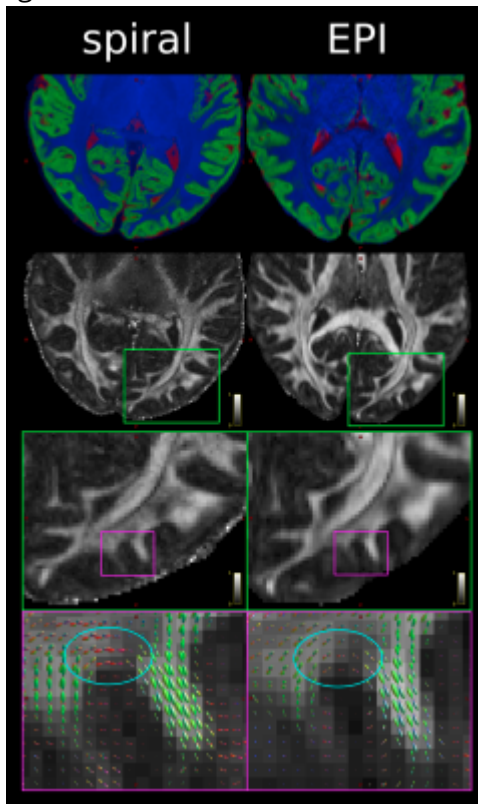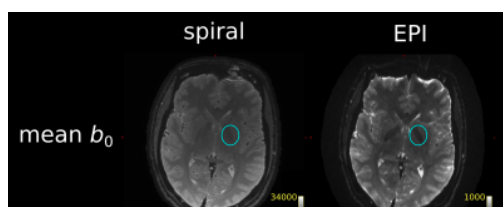
Figures

Figure 1: Comparison of spiral and EPI in the occipital lobe. Top: RGB segmentations of DWI data using multi-tissue CSD show better definition of the cortex in the spiral acquisition. Middle: Fractional anistropy (FA) maps further demonstrate the higher effective resolution of the spiral, i.e. less blurring. Bottom: fODFs seem to be more prominent for the iron-rich U-fibres connecting the two gyri (cyan ovals) in the spiral acquisition (short TE) than EPI (long TE). The same glyph scaling was used for both.
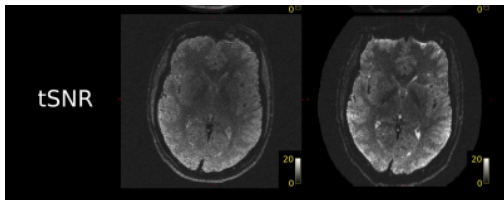
Figure 2: Spiral and EPI data show similar tSNR distributions. The anterior-left (top right of each figure panel) artefact is due to a fiducial oil capsule attached to the subject's forehead. The longer TR of the EPI acquisition resulted in higher cerebrospinal fluid (CSF) signal in the ventricles and near the surface of the brain. The contrast in the putamen (cyan ovals), an iron-rich deep grey matter structure, shows distinct differences between the spiral and EPI because of the different TEs.